Article

Cell PRESS

The Efficacy of siRNAs against Hepatitis C Virus Is Strongly Influenced by Structure and Target Site Accessibility

Selena M. Sagan,[1,3,]* Neda Nasheri,[1] Christian Luebbert,[1] and John Paul Pezacki[1,2,]*

[1]Steacie Institute for Molecular Sciences, The National Research Council of Canada, Ottawa, ON K1A 0R6, Canada
[2]Department of Biochemistry, Microbiology and Immunology, University of Ottawa, Ottawa, ON K1N 6N5, Canada
[3]Present address: Department of Microbiology and Immunology, Stanford University, Sherman Fairchild Building, Stanford, CA 94305-5124, USA
*Correspondence: smsagan@stanford.edu (S.M.S.), john.pezacki@nrc-cnrc.gc.ca (J.P.P.)
DOI 10.1016/j.chembiol.2010.04.011

SUMMARY

Hepatitis C virus (HCV) is a global health problem. Designing therapeutic agents that target HCV's RNA genome remains challenging. HCV genomic RNA is large and highly structured with long-range genome-scale ordered RNA structures. Predicting the secondary- and tertiary-structure elements that reveal the accessibility of target sites within HCV RNA is difficult because of the abundance of long-range interactions. Target site accessibility remains a significant barrier to the design of effective therapeutics such as small interfering RNAs (siRNAs) against different strains of HCV. Here we developed two methods that interrogate the folding of HCV RNA, an approach involving viral RNA microarrays (VRMs) and an HCV viral RNA-coated magnetic bead-based (VRB) assay. VRMs and VRBs were used to determine target site accessibility for siRNAs designed against the HCV genome. Both methods predicted potency of siRNAs in cell-culture models for HCV replication that are not easily predicted by informatic means.

INTRODUCTION

Hepatitis C virus (HCV) infection is a rapidly increasing global health concern, with over 200 million people infected worldwide. In most infected individuals, HCV establishes a chronic infection that can lead to cirrhosis, hepatocellular carcinoma, and death. Currently, there is no vaccine available and antiviral therapy, which consists of combination therapy with pegylated-IFNα 2a and ribavirin, achieves sustained response rates in only approximately 50% of infected patients (McHutchison et al., 2006). Although new antiviral agents are in development, the rapid development of resistance suggests that multiple drugs may be needed to limit the emergence of drug-resistant strains (Randall et al., 2003). There is thus an urgent need to develop effective preventative and alternative therapeutic strategies for HCV infection.

HCV is a positive-sense RNA virus that replicates through a double-stranded (ds) RNA intermediate in the cytoplasm of host cells. Its genome encodes an ∼3000 amino acid polyprotein which is cleaved, by host and viral proteases, into three structural proteins (core, E1, and E2) and seven nonstructural proteins (p7, NS2, NS3, NS4A, NS4B, NS5A, and NS5B). As for all RNA viruses, the positive-sense HCV RNA genome serves as a template for translation, negative-strand synthesis, and packaging into virions. A number of well-defined *cis*-acting RNA elements have been identified that mediate these processes during the HCV life cycle (Le et al., 1995; Tanaka et al., 1995, 1996; Wang et al., 1995; Wang and Siddiqui, 1995; Kolykhalov et al., 1996; Blight and Rice, 1997; Friebe et al., 2001, 2005; Friebe and Bartenschlager, 2002; Kim et al., 2002; Tuplin et al., 2002, 2004; Lee et al., 2004; You et al., 2004; McMullan et al., 2007; Diviney et al., 2008; You and Rice, 2008). In addition, Simmonds and colleagues have recently used increasingly advanced computational approaches to provide evidence for evolutionarily conserved, genome-scale ordered RNA structures (GORS) of yet unknown function within the genome of HCV and a number of other diverse RNA viruses from plants and animals (Simmonds, 2004; Davis et al., 2008). This suggests that target site accessibility may be an important factor when designing therapeutics that target these highly structured viral genomes, including small RNA species such as small interfering RNAs (siRNAs). HCV is a particularly attractive target for siRNA-based antiviral therapy because it is a cytoplasmically replicating, single-stranded RNA virus whose genome functions as both an mRNA and the template for viral replication.

The RNA silencing pathway uses the RNA-induced silencing complex (RISC) and siRNA duplexes to target complementary mRNAs for endonucleolytic cleavage (Fire et al., 1998; Zamore and Haley, 2005). It has recently been demonstrated that the folded state of the target mRNA can hamper the effectiveness of siRNAs considerably (Holen et al., 2002; Bohula et al., 2003; Kretschmer-Kazemi Far and Sczakiel, 2003; Vickers et al., 2003; Xu et al., 2003; Brown et al., 2005; Tafer et al., 2008; Watts et al., 2009). An innovative method called RNA*xs* has been developed in an attempt to address the issue of target site accessibility in mRNAs (Tafer et al., 2008); however, this method cannot account for the large amount of secondary structure present in the highly complex genomes of RNA viruses and has thus far been applied only to cellular mRNAs. Another innovative method
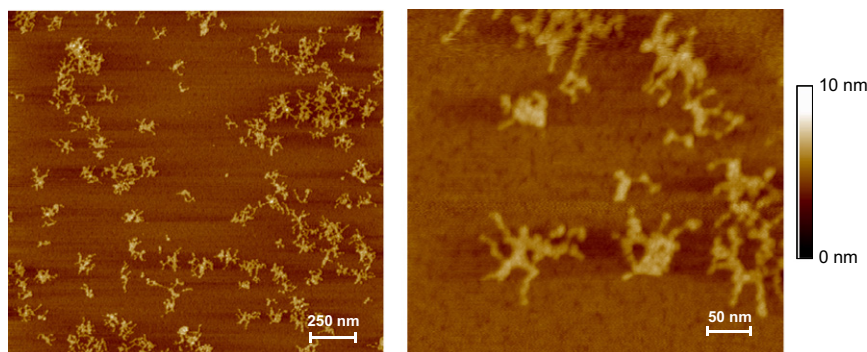
Figure 1. AFM of HCV RNA
HCV RNAs appeared as tightly packed clusters upon deposition, indicating that the tertiary interactions remain intact in the collapsed state. HCV RNAs had diameters of approximately 80–120 nm. The Z scale ranges from 0 to 10 nm.

employing high-throughput selective 2′-hydroxyl acylation analyzed by primer extension (SHAPE) was employed to characterize secondary-structure elements within the entire genome of HIV-1 (Watts et al., 2009). Watts et al. were able to correlate HIV-1 mRNA evolutionarily conserved structural elements with folded domains in their respective protein products, implying a role for the folding of genomic RNA in assisting with protein folding during translation (Watts et al., 2009). This approach, although highly innovative, is not designed for the interrogation of target site accessibility of siRNAs. In addition, HCV genomic RNA contains a larger amount of structured RNA or GORS than the HIV-1 genome (Simmonds et al., 2004; Davis et al., 2008).

In this study, we sought to investigate the importance of target RNA structure for the effectiveness of siRNAs directed against the highly structured HCV genome. We demonstrate that in vitro hybridization assays can be used to predict the effectiveness of HCV-specific siRNAs in cell culture. Our results suggest that target site accessibility may be a particularly important parameter for the design of effective siRNAs against the large, highly structured genomes of positive-sense RNA viruses, and have implications for the design and screening of highly effective siRNAs against such targets.
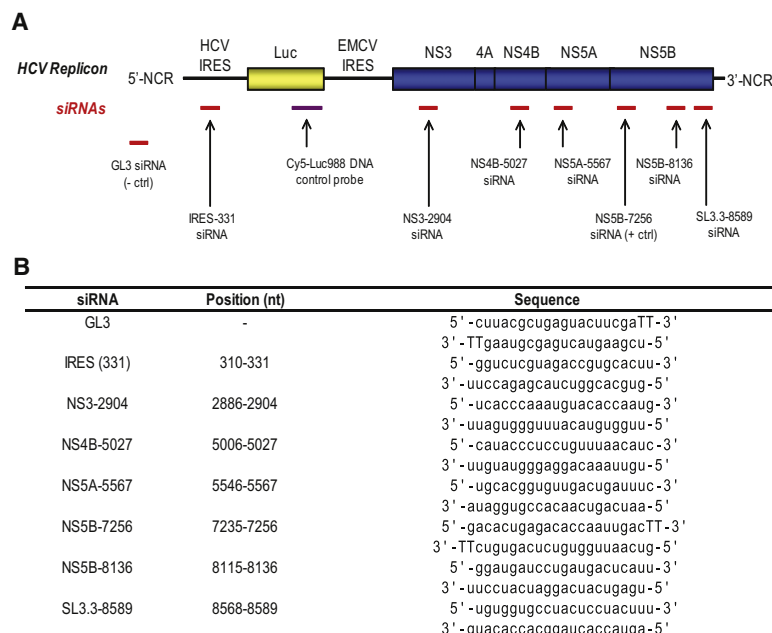
RESULTS

HCV Replicon RNA Retains a Complex Folded Structure upon Deposition

To investigate the physical nature of the highly structured HCV replicon RNA, HCV replicon RNA transcripts were directly visualized by atomic force microscopy (AFM). AFM has been extensively used in the study of DNA (Umemura et al., 2000; Hansma et al., 2004; Liu et al., 2005) and, more recently, has been extended to the investigation of large-scale secondary structure of RNAs (Drygin et al., 1998; Hansma et al., 1999, 2003, 2004; Giro et al., 2004; Alvarez et al., 2005; Kuznetsov et al., 2005; Noestheden et al., 2007; Davis et al., 2008). Upon imaging, the HCV replicon RNA transcripts uniformly adopted a tightly packed condensed state that was largely maintained during the deposition process (Figure 1). HCV replicon RNAs had a regular unit size with a mean radii for the x and y axes of approximately 30 nm and mean heights of 3.9 ± 1.0 nm (n = 10). This indicates that, under appropriate conditions, HCV replicon RNA can be spotted onto surfaces in a complex, highly folded conformation that may be representative of the native conformation.

Design of siRNAs against HCV Replicon RNA

Once it was demonstrated that the HCV replicon RNA could be spotted in a complex, highly folded conformation, we wanted to further investigate whether hybridization to spotted HCV replicon RNAs could be used to predict the potency of HCV replicon-specific siRNAs. Synthetic siRNAs were thus designed targeting different regions of the HCV replicon RNA (Figure 2). siRNAs were designed using the rules outlined by Reynolds and colleagues (Reynolds et al., 2004) and had similar G+C contents to ensure equal binding strengths irrespective of the overall base composition of the siRNAs (Figure 2). The siRNAs were named according to their nucleotide location in the subgenomic replicon RNA (Figure 2). As controls, two previously characterized HCV-specific siRNAs were used: IRES-331 siRNA directed against the HCV internal ribosomal entry site (IRES) region of the HCV replicon RNA (Yokota et al., 2003), and NS5B-7256 siRNA, a highly potent siRNA directed against the NS5B region of the replicon RNA (Wilson et al., 2003). As a negative control, GL3 siRNA was used, which has no sequence complimentarity to HCV replicon RNA. Finally, as a control for target site accessibility, an siRNA (SL3.3-8589) was designed against the 5′ arm of a known stem-loop region (SL3.3) in the NS5B open reading frame (You et al., 2004; Friebe et al., 2005). All siRNAs were fluorophore conjugated at the 5′ end of their antisense (guide) strands so that hybridization could be monitored by fluorescence.

Hybridization of siRNAs to Viral RNA Microarrays Is Restricted by Target Site Accessibility

To investigate the ability of hybridization to spotted HCV replicon RNA to differentiate between accessible and inaccessible target RNA sequences, we prepared viral RNA microarrays (VRMs). VRMs were prepared by spotting the HCV replicon RNA under native conditions on epoxysilane-coated glass slides. The target RNA was diluted in native spotting buffer and was printed in quadruplicate in increasing concentrations on the microarray from 5 to 500 ng/μl (Figure 3A). As negative and positive controls, oligonucleotides complementary to *Campylobacter jejuni* genes were spotted in duplicate (negative control) or quadruplicate (positive controls) in the microarrays at a concentration of 500 ng/μl (Figure 3A). The Cy3 channel (left) shows hybridization of the Cy3-labeled *C. jejuni* DNA controls and hybridization of the guide strand of NS5B-7256 siRNA to the HCV replicon RNA, whereas the Cy5 channel (right) represents hybridization of the Luc988-42 nt DNA control probe to the luciferase region of the HCV replicon RNA, which was used to normalize the data (Figure 3A).

A

B

siRNA	Position (nt)	Sequence
GL3	-	5'-cuuacgcugaguacuucgaTT-3' 3'-TTgaaugcgagucaugaagcu-5'
IRES (331)	310-331	5'-ggucucguagaccgugcacuu-3' 3'-uuccagagcaucuggcacgug-5'
NS3-2904	2886-2904	5'-ucacccaaauguacaccaaug-3' 3'-uuaguggguuuacaugugguu-5'
NS4B-5027	5006-5027	5'-cauacccuccuguuuaacauc-3' 3'-uuguauggggaggacaaauugu-5'
NS5A-5567	5546-5567	5'-ugcacgguguugacugauuuc-3' 3'-auaggugccacaacugacuaa-5'
NS5B-7256	7235-7256	5'-gacacugagacaccaauugacTT-3' 3'-TTcugugacucuguggguuaacug-5'
NS5B-8136	8115-8136	5'-ggaugauccugaugacucauu-3' 3'-uuccuacuaggacuacugagu-5'
SL3.3-8589	8568-8589	5'-uguggugccuacuccuacuuu-3' 3'-guacaccacggaucaccauga-5'

Figure 2. HCV-Specific siRNAs

(A) Schematic diagram of the HCV subgenomic replicon showing the approximate location of the HCV-specific siRNAs (red). The Cy5-labeled Luc988-42 nt DNA control probe location is indicated in purple.

(B) HCV-specific siRNA sequences and their positions in the HCV subgenomic replicon RNA.

hybridized in triplicate. The positive-control NS5B-7256 siRNA gave the highest signal intensity, whereas the negative-control GL3 siRNA, with no sequence complementarity to the HCV replicon RNA, had negligible signal intensity similar to background (see Hyb Buffer, Figure 3C). The NS5B-8136, NS5A-5567, and NS3-2904 siRNA had the next highest signal intensities, with normalized net intensities 78.7%, 72.6%, and 62.2% of the positive-control NS5B-7256 siRNA, respectively. This was followed by the negative control for target site accessibility, SL3.3-8589 siRNA (49.2%), and the NS4B-5027 siRNA (30.3%). The low signal intensity of the NS4B-5027 siRNA suggests that this siRNA may be directed against an inaccessible target site within the HCV replicon RNA.

In order to establish whether VRMs could be used to distinguish between accessible and inaccessible targets, hybridization of the positive- and negative-control single-stranded fluorophore-labeled antisense (guide) siRNAs was carried out under native and denaturing conditions (Figure 3B). Under native conditions, regions of the HCV replicon RNA with a high degree of stable internal base pairing should adopt a closed configuration and be relatively inaccessible to guide strand hybridization. In contrast, the relatively unstructured regions of the HCV replicon RNA should be relatively accessible and lead to a greater degree of hybridization. Under denaturing conditions, the inaccessible regions should become unpaired, resulting in an open conformation that should have a similar degree of hybridization to the accessible regions. The NS5B-7256 siRNA has previously been described as a highly potent siRNA against HCV replicon RNA (>90% reduction in HCV replicon RNA 72 hr posttransfection) (Wilson et al., 2003); as such, it is likely to have a highly accessible target within the HCV replicon RNA. In agreement with this, hybridization of this siRNA guide strand to the VRMs yielded similar normalized net intensities under native and denaturing conditions (Figure 3B). In contrast, the SL3.3-8589 siRNA, designed against the 5′ arm of a known stem-loop region (SL3.3) in the HCV replicon RNA (You et al., 2004; Friebe et al., 2005), should be largely inaccessible to hybridization. Under native conditions, the normalized net intensities of SL3.3-8589 siRNA guide-strand hybridization were approximately 40% of that observed under denaturing conditions (Figure 3B), suggesting that hybridization of guide-strand siRNAs to the VRMs is restricted by target site accessibility under native conditions.

Using the VRMs, the accessibility of all of the HCV-specific siRNA guide strands was analyzed by quantifying their hybridization under native conditions (Figure 3C). Hybridization intensities of the different siRNAs were scaled according to standard amounts of DNA oligonucleotide controls to give the normalized net intensities, and all siRNA guide strands were

Hybridization of siRNAs to VRBs Is Restricted by Target Site Accessibility

To further demonstrate that hybridization of guide-strand siRNAs to HCV replicon RNA under native conditions is restricted by target site accessibility, we extended our hybridizations to a solution-based approach more representative of the situation in vivo. The HCV replicon RNA was first end labeled with maleimide-PEG11-biotin and then hybridized to fluorophore-conjugated siRNAs under native or denaturing conditions in solution. The hybridized HCV replicon RNA was then captured on streptavidin-coated magnetic microbeads and imaged using fluorescence microscopy to assess target site accessibility (Figure 4A). The HCV-specific siRNAs were hybridized in increasing concentrations under native and denaturing conditions. To account for any nonspecific binding of the siRNAs to the beads, reactions were also carried out in the absence of HCV replicon RNA. Representative images from each of the siRNA hybridizations are shown in Figure 4B.

Quantification of signal intensities from individual beads per image (n = 100) using increasing concentrations of siRNAs (10 nM to 1 μM) was used to generate line graphs for siRNAs during native and denaturing hybridizations (Figure 5A). The net integrated optical density (IOD) of SL3.3-8589 siRNA guide-strand hybridization was approximately 18% of that observed under denaturing conditions, whereas the net IOD of the NS5B-7256 siRNA guide strand was largely unchanged under native and denaturing conditions (Figure 5B). This suggests that, like the VRMs, hybridization of guide-strand siRNAs to viral RNA-coated magnetic bead-based (VRB) assays is restricted by target site accessibility under native conditions.
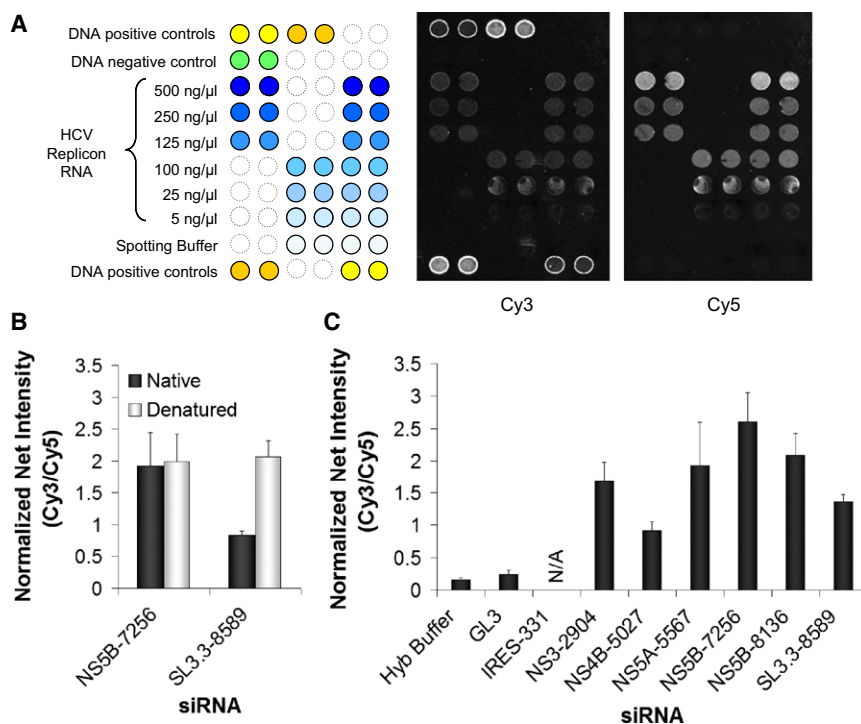
Figure 3. Viral RNA Microarrays

(A) Schematic diagram of the VRM design and a representative VRM hybridization. After hybridization of HCV-specific siRNAs, slides were scanned using a microarray scanner, resulting in images of the siRNA and DNA positive controls in the Cy3 channel (middle) and the Luc988-42 nt control probe in the Cy5 channel (right) that were used in the normalization of the microarray data. A representative hybridization of NS5B-7256 siRNA is shown.

(B) Hybridization to VRMs under native and denaturing conditions. The normalized net intensities (Cy3/Cy5) of the positive-control NS5B-7256 siRNA and the negative-control SL3.3-8589 siRNAs are shown. Error bars represent SE.

(C) Hybridization of the HCV-specific siRNAs to VRMs under native conditions. The data represent the average of two independent hybridizations, and normalized net intensities (Cy3/Cy5) from a single HCV replicon RNA concentration (125 ng/μl) are shown. Error bars represent SE.

The accessibility of all of the HCV-specific siRNA guide strands was analyzed by quantifying their hybridization to the HCV replicon RNA in solution under native and denaturing conditions (Figure 5C). The net IODs from the image analyses were used to generate curves of the native and denaturing hybridizations for each siRNA. The ratio of the slope of the native hybridization to the denatured hybridization for each siRNA was used as a measure of target site accessibility (Figure 5C). The positive-control NS5B-7256 siRNA gave the highest signal intensity, with a ratio of 0.87 ± 0.16, whereas the negative-control GL3 siRNA, with no sequence complementarity to the HCV replicon RNA, had negligible signal similar to background (0.008 ± 0.001; Figure 5C). The NS5B-8136 and NS3-2904 siRNAs had the next highest ratios, with ratios of 0.75 ± 0.08 and 0.77 ± 0.13, respectively. The NS5A-5567 and IRES-331 siRNAs had intermediate signals, with ratios of 0.36 ± 0.12 and 0.25 ± 0.06, respectively. Finally, the NS4B-5027 and SL3.3-8589 had low signal intensities, with ratios of 0.21 ± 0.06 and 0.15 ± 0.08, respectively (Figure 5C). The intermediate and low signal intensities likely represent intermediate accessibility of the siRNA target sites within the native HCV replicon RNA structure.

Prediction of siRNA Potency Based on Target Site Accessibility Correlates with siRNA Knockdown in Cell Culture

To correlate the target site accessibility predictions from the VRMs and VRBs to siRNA knockdown in cell culture, the effect of each of the HCV-specific siRNAs on HCV protein and replicon RNA levels was examined by western and northern blot analyses from siRNA duplex transfection of Huh-7 cells stably harboring HCV subgenomic replicon RNA (Figures 6A and 6B). The levels of the HCV NS5A protein correlated well with the amount of

HCV replicon RNA, suggesting that the siRNAs are functioning by an RNA cleavage-based mechanism rather than translational repression in cell culture.

For a more quantitative approach to assessing siRNA knockdown, we used quantitative real-time polymerase chain reaction (qPCR) analyses to quantify the levels of HCV replicon RNA after siRNA duplex treatment of Huh-7 cells stably harboring HCV subgenomic replicon RNA (Figure 6C). Treatment with interferon γ (IFNγ) served as a positive control for knockdown of HCV replicon RNA, reducing the levels of the HCV replicon RNA ∼6.7-fold compared to mock-treated samples. The NS3-2904, NS5B-7256, and NS5B-8136 siRNAs all reduced HCV replicon RNA levels to a similar degree, with mean fold reductions of 5.1-, 4.9-, and 5.0-fold, respectively (Figure 6C). The IRES-331 and NS5A-5567 siRNAs had intermediate knockdowns of 2.5- and 2.2-fold, respectively, whereas the NS4B-5027 and SL3.3-8589 siRNAs both reduced HCV RNA levels by only 1.5-fold (Figure 6C). The negative-control (GL3) siRNA did not have a significant effect on the levels of the HCV NS5A protein (Figure 6A) or the replicon RNA (Figures 6B and 6C), indicating that the effects of the siRNAs on HCV protein and RNA levels are sequence specific and are not caused by induction of the nonspecific IFN response. This is consistent with other findings that dsRNAs < 30 nt do not induce significant IFN responses (Minks et al., 1979; Manche et al., 1992). Thus, the effects of the designed siRNAs on HCV protein and RNA levels seem to be the result of siRNA-directed degradation of HCV replicon RNA by HCV-specific siRNA-loaded RISC.

DISCUSSION

Spotting HCV Replicon RNA in a Native Conformation for VRMs

The high resolution possible with AFM provides a means to directly visualize deposited HCV replicon RNA at the molecular
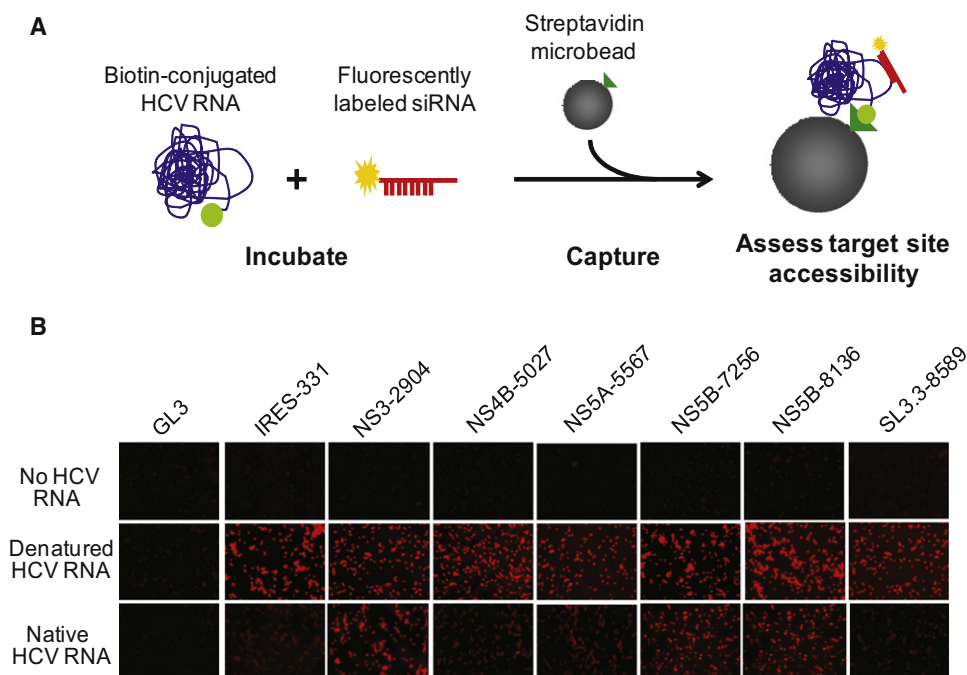
Figure 4. Viral RNA Beads

(A) Schematic diagram of hybridization of siRNAs to biotin-conjugated HCV replicon RNA and capture on magnetic microbeads. Biotin-labeled HCV replicon RNAs are first incubated under native or denaturing conditions with fluorophore-conjugated siRNAs. The hybridized siRNAs are then captured on magnetic streptavidin-conjugated microbeads. The beads are washed and then target site accessibility is assessed by fluorescence microscopy.

(B) Representative fluorescence images of VRBs after hybridization with 100 nM siRNAs under native and denaturing conditions. "No HCV RNA" represents hybridization reactions carried out in the absence of HCV replicon RNA in order to assess nonspecific binding of the siRNAs to the beads.

level (Rivetti et al., 1996; Hansma et al., 2003; Alvarez et al., 2005; Kuznetsov et al., 2005; Noestheden et al., 2007). Previous studies have used AFM analyses to visualize specific RNA-RNA interactions such as kissing-loop interactions (Hansma et al., 2003) or RNA virus genome circularization (Alvarez et al., 2005) and, more recently, we and others have used it to visualize the larger-scale shape of RNA molecules (Kuznetsov et al., 2005; Noestheden et al., 2007; Davis et al., 2008). We have previously demonstrated that HCV RNA exhibits more complex tertiary structure than other RNA virus genomes, as measured by AFM (Davis et al., 2008). In the current study, it was demonstrated that HCV RNA can be spotted in a very regular, tightly packed condensed state (Figure 1).

Despite the high resolution of this technique, AFM does introduce artifacts associated with the deposition process, most notably the flattened appearance of the RNAs (i.e., the measured x and y diameters are approximately 15 times greater than their height) (Rivetti et al., 1996; Hansma et al., 2003; Davis et al., 2008). This is likely due to the partial dissolution of the condensed state resulting from interactions with surface divalent metal ions during drying of the samples (Noestheden et al., 2007; Davis et al., 2008). Nevertheless, the AFM imaging revealed a regular, tightly packed condensed structure of the HCV replicon RNA with many of the tertiary structures remaining intact, despite the shape distortions that likely arise during AFM.

VRMs and VRBs Are Restricted by Target Site Accessibility

Traditional microarray experiments are based on duplex stability (thermodynamics) between the nucleic acid probe and its target. They are typically carried out close to the melting temperature of the specific nucleic acid probe-target interaction under conditions which destroy the less-stringent secondary structures that may be present in the target. The VRMs described herein differ from traditional microarrays in that they are carried out under native conditions meant to preserve the secondary and tertiary structure of the target RNA. In this way, VRMs are a measure of hybridization speed (kinetics) of the siRNA-target interaction and reflect the accessibility of the folded state of the RNA target.

Hybridization of HCV-specific guide-strand siRNAs to HCV VRMs was used as a measure of target site accessibility. Using the control siRNAs, we were able to demonstrate that hybridization to the VRMs under native conditions was restricted by target site accessibility (Figure 3B). This was also reflected in the hybridization studies carried out in solution, on VRBs, which may more closely represent the native environment of the HCV replicon RNA in vivo (Figures 5A and 5B). Hybridization of the whole panel of HCV-specific siRNAs demonstrated that the NS3-2904, NS5B-7529, and NS5B-8136 siRNAs had relatively high hybridization intensities under native conditions, suggesting their target sites are likely to be relatively accessible in the native HCV replicon RNA (Figures 3C and 5C). The NS5A-5567 siRNA
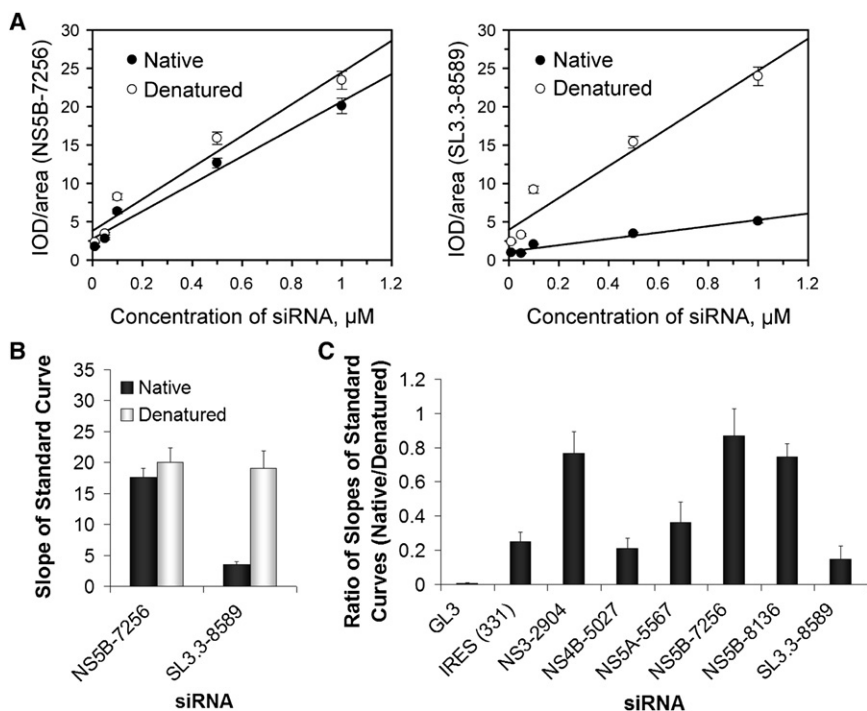
Figure 5. VRB Data Analysis

(A) Quantification of net IODs from individual beads (n = 100) from images of increasing siRNA concentrations was used to generate line graphs of signal intensities under native (closed circles) and denaturing (open circles) conditions. Line graphs of the positive-control NS5B-7256 (left) and negative-control SL3.3-8589 (right) siRNAs are shown. Error bars represent SE.

(B) Hybridization to VRBs under native and denaturing conditions. The slopes of the standard curves generated in (A) were used to generate a bar graph of the positive-control NS5B-7256 and negative-control SL3.3-8589 siRNA hybridizations to the VRBs under native and denaturing conditions. Error bars represent SE.

(C) Ratio of slopes from native and denaturing hybridization of the HCV-specific siRNAs to VRBs. The data represent the average of three independent hybridizations, and net IODs from image analyses were used to calculate the slopes for native and denaturing hybridizations. Error bars represent SD of at least three independent replicates.

had intermediate intensity, whereas the IRES-331 and NS4B-5027 siRNA had relatively low hybridization intensities similar to that of the SL3.3-8589 siRNA. This suggests that in addition to the IRES-331 and SL3.3-8589 siRNAs that are directed against known structured regions in the HCV genome, NS4B-5027 is also likely to have a relatively inaccessible target site within the native HCV replicon RNA (Figures 3C and 5C).

The minimal hybridization seen with the NS4B-5027 siRNA is likely to be due to the highly structured nature of HCV replicon RNA. Alternatively, it cannot be ruled out that the apparent inaccessibility of this siRNA could be a result of a "shell" of folded RNA shielding an unfolded core of unstructured RNA within the 3D conformation of the RNA. However, Simmonds and colleagues have previously investigated this possibility for the HCV RNA genome in their investigation of GORS (Davis et al., 2008). By creating chimeric viral RNAs where a region of the relatively unstructured Bunyavirus (BV) RNA (non-GORS) was inserted into the HCV viral RNA (GORS), they were able to demonstrate that insertions into the RNA genome did not affect the accessibility of the surrounding regions to probe hybridization (Davis et al., 2008). The same was true for the reverse chimera (i.e., where regions of the HCV RNA genome were inserted into the BV RNA genome), arguing against the shell hypothesis (Davis et al., 2008).

The results obtained from the VRMs and VRBs qualitatively correlate with one another, validating our hypothesis that the spotting of HCV RNA under native folding conditions mimics the native, folded state in solution (measured by VRBs). The advantages of using both VRMs and VRBs are that these approaches are high throughput and have the capacity to be adapted to other RNA viruses as well as other nucleic acid interactions, and that they involve the use of small quantities of

reagents and rapidly result in empirical data on target site accessibility. The additional advantage of using VRBs is that they are likely more representative of the true folded state, unencumbered by surface effects that might arise during spotting and hybridization procedures on the surface of glass slides.

Correlating Target Site Accessibility to Silencing in Cell Culture

The results from hybridizations to VRMs and VRBs largely correlated with the potency of the siRNAs in cell culture (Figure 7). The pattern of potency of the siRNAs is unlikely to be due to the kinetics of silencing because western and northern blots prepared from 24, 48, and 72 hr posttransfection resulted in similar patterns of siRNA silencing (data not shown). The HCV-specific siRNAs with high target site accessibility tended to silence HCV protein expression and replicon RNA levels quite efficiently, whereas those predicted to be target inaccessible by in vitro hybridization tended to have little effect on HCV protein and replicon RNA levels (Figure 6). This is despite the fact that in both cases the composition of the hybridization buffer does not reflect the protein-rich cytosolic environment of the cell. In the future, it will be interesting to include host or viral proteins in the hybridization reactions to identify specific protein-RNA interactions.

Implications for siRNA Design

Many factors contribute to the overall efficiency of RNA silencing. The majority of available siRNA design software use eight parameters that, when incorporated into a rational siRNA design algorithm, increase the probability of selecting an effective siRNA (i.e., one capable of silencing gene expression by >50%) (Elbashir et al., 2002; Reynolds et al., 2004). These
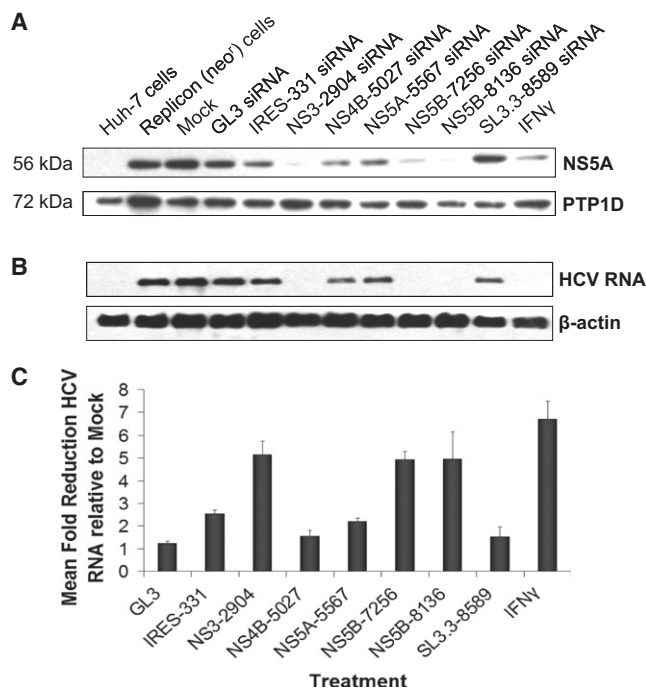
A

B

C

Figure 6. Analysis of siRNA Knockdown in Cell Culture

(A) Western blot analysis of HCV NS5A protein levels in HCV subgenomic replicon-harboring cells 48 hr posttransfection with HCV-specific siRNAs. Samples from the parental Huh-7 cells (lane 1) and replicon-harboring cells (lane 2) are shown. Mock-transfected samples (lane 3, transfection reagent only) and samples transfected with the negative-control (GL3, lane 4) and HCV-specific siRNAs (lanes 5–11) are shown. IFNγ was used as a positive control for knockdown of HCV NS5A protein and replicon RNA.

(B) Northern blot analysis of HCV replicon RNA levels in HCV subgenomic replicon-harboring cells 48 hr posttransfection with HCV-specific siRNAs. The samples analyzed by northern blot are identical to those described for (A).

(C) qPCR analysis of siRNA knockdown in cell culture. Data are represented as mean fold reduction in HCV replicon RNA relative to mock-treated samples. Experimental replicates were performed in triplicate and error bars represent SD.

include a G+C content between 30% and 52% (Elbashir et al., 2002; Holen et al., 2002; Reynolds et al., 2004), low internal stability of the 3′ terminus of the sense (passenger) strand (Khvorova et al., 2003; Schwarz et al., 2003; Reynolds et al., 2004), lack of internal repeats (Reynolds et al., 2004), an A base at position 19 (sense strand), an A base at position 3 (sense strand), a U base at position 10 (sense strand), a base other than G or C at position 19 (sense strand), and a base other than G at position 13 (sense strand) (Elbashir et al., 2002; Reynolds et al., 2004). In these algorithms, the only measure of target site accessibility is based on G+C contents, as G+C contents of 30%–64% have been demonstrated to correlate with accessibility (Elbashir et al., 2002; Reynolds et al., 2004); however, relying on G+C content alone results in a large number of predicted false negatives (Heale et al., 2005).

In this study, despite a rational approach to siRNA design, only a fraction of the siRNAs were effective at reducing the expression of the HCV replicon RNA, with the efficiency of the different siRNAs varying significantly. The efficiency of knockdown in cell culture did not correlate with any of the parameters outlined by

Reynolds and colleagues (Reynolds et al., 2004), including melting temperature or G+C content. Additional parameters must therefore affect the efficiency of siRNAs for HCV knockdown.

Efficiency of loading into the RISC could also potentially contribute to differences in silencing efficiency of HCV-specific siRNAs (MacRae et al., 2008). To investigate this possibility, we explored the ability of recombinant human argonaute 2 (hAGO2) to load the HCV-specific siRNAs in vitro. The majority of the siRNAs were efficiently loaded into hAGO2 after a 30 min incubation period (>75% for seven of the eight siRNAs) and the slight variations in loading did not correlate with silencing efficacy, arguing against the efficiency of RISC loading as a contributing factor to silencing efficiency in this case. However, the contribution of other cellular RNA silencing pathway components to the efficiency of RISC loading cannot be ruled out within the complex environment of the cell. Nevertheless, due to the rational design of the siRNAs with similar G+C contents, it is unlikely that there are dramatic differences in the ability of RISC to unwind the siRNA duplexes in cell culture.

A few groups have now described algorithms that take into account local secondary-structure prediction in siRNA design that have improved the probability of designing effective siRNAs (Heale et al., 2005; Overhoff et al., 2005; Tafer et al., 2008; Varekova et al., 2008). However, for long RNA targets, the prediction accuracy of currently available computational algorithms is still very low, generating numerous alternative structures (Luo and Chang, 2004; Schubert et al., 2005). In addition, the prevalence of long-range RNA-RNA interactions in the genomes of RNA viruses is not yet amenable to accurate modeling. In order to test the ability of secondary-structure prediction to predict the accessibility of the siRNA targets in HCV replicon RNA, we carried out phylogenetic covariation analyses by folding energy scans of the 83 available HCV 1b sequences using Simmonic (Simmonds et al., 2004; Davis et al., 2008), which utilizes UNAfold for prediction of secondary structure (Markham and Zuker, 2005) (Figure 7). We carried out our analyses on all of the known HCV genotype 1b sequences rather than just the HCV replicon RNA used in this study, as the homologous genotype 1b RNAs are similar enough to form the same structure but exhibit polymorphisms which can be informative. Mean free energy of folding difference (MFED) scores of the siRNA target sites and the regions 30 nt adjacent to them did not correlate with their knockdown efficiencies (Figure 7). In fact, the NS5B-8136 siRNA was predicted to target a relatively structured region although it was one of the most potent siRNAs in cell culture (Figure 6). Hence, reliable results of analyses based on computational secondary-structure prediction cannot be guaranteed for such targets (Luo and Chang, 2004).

The native hybridization-based methods described herein thus represent a rapid high-throughput approach to screening for effective siRNAs against the highly structured HCV RNA genome and has the potential to be applied to other RNA-RNA interactions, including the genomes of other highly structured positive-sense RNA viruses. Although we only investigated interactions with the Con1 HCV 1b genomic sequence in this study, the high-throughput nature of this approach makes it easy to apply it to all 83 known clinical variants of the HCV genotype
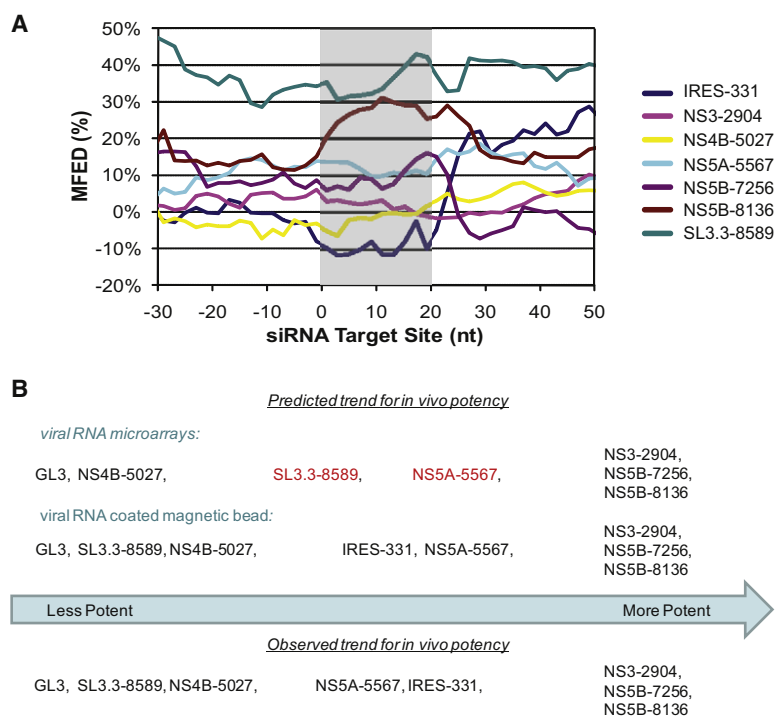
A

B

Figure 7. Analysis of HCV-Specific siRNA Target Sites

(A) Distribution of MFEDs across the siRNA target sites and the adjacent 30 nt based on folding energy scans of the 83 published HCV genotype 1b sequences available in GenBank. Mean MFEDs (% difference in MFEs of the native and scrambled sequences) for the individual siRNA target sites were calculated based on folding energy scans of aligned sequences for consecutive 150-base fragments (in 2-base increments). Large MFEDs indicate the target sequence is more structured than the null expectation. siRNA target sites are shaded in gray (nt 1–21), where 1 represents the first nucleotide of the siRNA target site.

(B) Schematic showing the predicted versus actual potency of eight different siRNAs. The horizontal arrow from left to right indicates relative potency. The predicted potencies lie above the arrow whereas the observed potencies are located below the arrow, with the least potent siRNAs on the left and most potent siRNAs on the right.

1b genomic sequences, or to other HCV genotypes and thus give broader target site accessibility information. The latter approach could assist in evaluating target site accessibility in highly conserved regions of the viral genome that may not be tolerant of escape mutations.

During natural infections, the HCV RNA genome is likely to have a dynamic structure able to readily accommodate unwinding, elongation, and exposure to different regions of the RNA to viral and cellular proteins for translation and replication of the viral genome. As a future direction, it may be interesting to examine how specific viral or cellular proteins affect the accessibility of the HCV replicon RNA in vitro. Addition of purified viral or cellular proteins or extracts to the in vitro hybridization reactions could yield new information about direct interactions with the viral genome. For example, addition of siRNA-hAGO2 complexes could help us gain information on the accessibility of the HCV RNA to the larger RISC rather than just the siRNA itself. The addition of viral proteins could help identify novel RNA-interacting domains such as packaging signals, which have yet to be identified for HCV. The VRB approach may be more amenable to addition of proteins, as it can avoid the surface effects that might result in conformational restriction of protein-RNA interactions that can occur in the VRM approach.

The results presented here and elsewhere clearly demonstrate that target RNA secondary structure has major consequences for siRNA-induced gene silencing (Holen et al., 2002; Bohula et al., 2003; Kretschmer-Kazemi Far and Sczakiel, 2003; Vickers et al., 2003; Xu et al., 2003; Brown et al., 2005). Recent studies have demonstrated that the structure of target RNA or the binding of proteins can also dramatically affect microRNA (miRNA) recognition of RNA targets (Hofacker, 2007; Kedde et al., 2007; Kertesz et al., 2007; Long et al., 2007; Obernosterer

et al., 2008). Because miRNA-target recognition is thought to require as little as 7 nt for targeting (Lewis et al., 2003), hybridization of miRNAs to VRMs or VRBs may also be useful for elucidation of the rules governing miRNA target site recognition as well as conformation of bona fide miRNA target sites.

Information gained from structural probing by native hybridization of nucleic acids may also serve as a starting point for the design of nucleic acid-based probes to pull down or titrate out novel interacting partners with the viral RNA genome. For example, where the hybridization of the siRNA probes in vitro disagrees with the silencing efficiency in cell culture, this may indicate that the siRNA target site is occupied by a novel protein-RNA or RNA-RNA interaction in vivo. RNA-based probes could then be designed to pull down or titrate out the interacting partners in the context of viral replication. RNA-based probes have already been demonstrated to be useful for elucidating protein-RNA or RNA-RNA interactions in a number of cellular systems (Srisawat and Engelke, 2002; Martinez et al., 2002). The VRM and/or VRB approaches could also be extended to other RNA molecules, including cellular mRNAs or the RNA genomes of other important human pathogens.

SIGNIFICANCE

Under appropriate conditions, the HCV replicon RNA can be spotted onto surfaces in a conformation that appears to be representative of the native conformation. Using hybridization to native HCV replicon RNA on surfaces or in solution, hybridization efficiency (target site accessibility) of HCV-specific siRNAs was correlated to silencing in cell culture. The parallels observed between in vitro hybridization and siRNA efficiency suggest that structured RNA elements in HCV replicon RNA is a major factor in determining the efficiency of synthetic siRNAs. The technique described here represents a rapid, high-throughput approach to screen for effective siRNAs directed against the large, highly structured HCV replicon RNA genome based on target site

accessibility. **This technique also has the potential to be extended to other RNA-RNA interactions, including the highly structured genomes of other important human pathogens and in the investigation of protein-RNA and RNA-RNA interactions.**

EXPERIMENTAL PROCEDURES

Cell Culture and HCV Replicons

The Huh-7 cell lines used in this study were cultured in Dulbecco's modified Eagle's medium (Invitrogen) supplemented with 100 nM nonessential amino acids, 50 U/ml penicillin, 50 μg/ml streptomycin, and 10% fetal bovine serum (PAA Laboratories). G418 (Geneticin) was added at a concentration of 250 μg/ml to the Huh-7 cells stably expressing HCV subgenomic replicons. The pFK-I389neo/NS3-3′/5.1 and pFK-I389luc/NS3-3′/5.1 plasmids, which contain HCV subgenomic replicons (genotype 1b, Con1, GenBank accession number AJ242654), were kindly provided by Ralf Bartenschlager (Institute of Hygiene, University of Heidelberg) (Lohmann et al., 1999). The replicons harbor either neomycin resistance (neo[R]; pFK-I389neo/NS3-3′/5.1) or the firefly luciferase (luc; pFK-I389luc/NS3-3′/5.1) gene at the 5′ end (driven by the HCV IRES), but otherwise are identical and express the HCV nonstructural proteins (NS3 to NS5B) from the encephalomyocarditis virus IRES as described in Lohmann et al. (1999).

For siRNA transfections, Huh-7 cells harboring the subgenomic replicon (pFK-I389neo/NS3-3′/5.1) were seeded in 60 mm dishes (1 × 10^{6} cells) for preparation of whole-cell lysates and total RNA extractions. The fluorescently labeled (Cy3 or Dy547) siRNA duplexes (10–100 nM; described below) were transfected using Lipofectamine RNAiMAX Transfection Reagent (Invitrogen) according to the manufacturer's protocol. Whole-cell lysates and RNA extractions were prepared at 24, 48, and 72 hr posttransfection. IFNγ was used as a positive control for knockdown of HCV RNA replication at a concentration of 100 U/ml.

siRNA Sequences

HCV-specific siRNAs were designed based on the HCV subgenomic replicon (GenBank accession number AJ242654) (Lohmann et al., 1999). The siRNA design software described in Yiu et al. (2005) was used for the design of HCV-specific siRNAs and is freely available at http://i.cs.hku.hk/~sirna/software/sirna.php. This software compiles the design software of Ambion, Jack, Emboss, MPI, Genscript, QIAGEN, Invitrogen, Deqor, and MPI + Rational for siRNA design. The organism that was selected was *Homo sapiens* and output siRNAs were selected that were predicted from at least four kinds of software. The top siRNAs were selected for further analysis and were scored according to the design criteria outlined by Reynolds and colleagues (Reynolds et al., 2004). The siRNAs that were selected for analysis had scores ≥ 6. The siRNA sequences used to investigate target site accessibility are listed in Figure 2. Where indicated, duplex siRNAs were formed between the corresponding sense and antisense strands according to the manufacturer's protocol. The IRES-331 siRNA and the positive control, NS5B-7256 siRNA (also known as NS5B-6367; Wilson et al., 2003), have been previously reported to be functional siRNAs for inhibition of HCV RNA in cell culture (Wilson et al., 2003; Yokota et al., 2003; Wilson and Richardson, 2005). The SL3.3-8589 siRNA was designed against a known stem loop in the NS5B coding region of the HCV genome (SL3.3; You et al., 2004; Friebe et al., 2005) as a negative control.

In Vitro Transcription

In vitro transcripts were generated using the MEGAscript T7 kit (Ambion) according to the manufacturer's protocol. Briefly, the template DNA was linearized with the restriction enzyme ScaI (New England Biolabs), precipitated for less than 30 min, and resuspended in RNase-free water to a final concentration of 0.5 μg/μl. The in vitro transcription reaction was set up in a final volume of 20 μl and incubated at 37°C for 4 hr. In order to degrade the template DNA, 1 μl of DNase I was added and the reaction was incubated for an additional 15 min at 37°C. The in vitro transcripts were then cleaned up using the MEGAclear kit (Ambion) according to the manufacturer's protocol. The concentration was determined by measurement of the absorbance at

260 nm with an ND-1000 spectrophotometer (NanoDrop Technologies), and RNA integrity was verified by electrophoresis using an Agilent 2100 bioanalyzer with the RNALabChip kit (Agilent Technologies) according to the manufacturer's protocol.

For VRBs, HCV subgenomic replicon RNA transcripts were biotinylated at the 5′ end using the 5′-EndTag nucleic acid labeling system (Vector Laboratories) according to the manufacturer's protocol. The EZ-Link maleimide-PEG11-biotin label (Thermo Fisher Scientific; 20 mM) was dissolved in RNase-free dimethyl sulfoxide (Sigma-Aldrich) and the final reaction volume was 20 μl. Labeled HCV subgenomic replicon RNA was then purified using the MEGAclear kit (Ambion), and the RNA integrity was verified by agarose gel electrophoresis and quantified by measurement of the absorbance at 260 nm with an ND-1000 spectrophotometer (NanoDrop Technologies).

Atomic Force Microscopy

RNA transcripts were diluted in AFM imaging buffer (20 mM HEPES, 10 mM MgCl₂, 3 mM NiCl₂ [pH 7]) to 0.5–2 ng/μl. Prior to RNA deposition, freshly cleaved mica (grade V2; Ted Pella) was treated with 4 mM NiCl₂ for 1 min at room temperature and washed twice by soaking in 10 ml nuclease-free water for 10 and 1 min, respectively. The NiCl₂-treated mica was then dried under a stream of nitrogen. Ten microliters of diluted RNA was dropped on the surface of the NiCl₂-treated mica and allowed to adsorb for 5 min at room temperature. Nonadsorbed RNA was removed by two washes with 10 ml of nuclease-free water, after which the sample was dried under a stream of nitrogen and imaged. Imaging was performed at room temperature (22 ± 1°C) on a PicoSPM atomic force microscope (Molecular Imaging) in acoustic mode using aluminum-coated silicon tips with spring constants of ~40 N/m and resonance frequencies between 250 and 325 kHz. Fields of 0.5–3.0 μm were scanned at 1–1.5 Hz. Images were flattened, and approximate cluster diameters were determined using PicoScan 5.3.3 software (Molecular Imaging). Three independently prepared samples were imaged for the HCV subgenomic replicon RNA transcript, and several areas were scanned for each sample.

VRM Design

A prototype microarray was generated consisting of a dilution series of HCV subgenomic replicon RNA (5, 25, 100, 125, 250, and 500 ng/μl) as well as *C. jejuni* positive- (Cj0373: 5′-GTA TCC ACG CAC CTT TAA ATG AAA AAA CC-3′; Cj1119c: 5′-GTA CCA TCG CTA TAA CTT TGG CTT-3′) and negative- (Cj1437c: 5′-GCC AGA GTG TAT GTG ATT TGG TTG AAC-3′) control oligonucleotides. Computer-based homology searches using NCBI BLAST were used to ensure that control oligonucleotides contained no homology with the *H. sapiens* or HCV genomes, or any of the HCV-specific siRNAs. All oligonucleotides were PAGE purified (Invitrogen) and spotted at a final concentration of 500 ng/μl. Each sample was spotted in quadruplicate, interspersed by blank spots across the array in order to reduce spatial effects (see Figure 3).

Preparation of VRM Oligonucleotide Controls

Cy3-labeled short DNA oligonucleotides complementary to the Cj1119c and Cj0373 oligonucleotides spotted on the microarrays were prepared as positive controls and printing quality controls using the Mirus Label-IT Cy3 labeling kit (Fisher Scientific) according to the manufacturer's protocol. For normalization purposes and to account for spot morphology, a DNA probe was designed against the relatively unstructured luciferase region of the HCV replicon. The Luc988-42 nt probe (5′-GGA AGG GCC ACA CCC TTA GGT AAC CCA GTA GAT CCA GAG GAA-3′) was labeled with Cy5 for cross-channel normalization, using the Mirus Label-IT Cy5 labeling kit (Fisher Scientific). All labeling reactions were carried out according to the manufacturer's protocol with the following modifications. Labeling reactions typically contained 5 μg DNA and 2.5 μl Cy3 or Cy5 label in a 50 μl reaction volume. Reactions were incubated at 37°C overnight. Unincorporated dye was removed by ethanol precipitation and the Cy3-labeled oligonucleotides were resuspended in RNase-free water. Labeling efficiencies were between 9 and 20 pg/μl as assessed using an ND-1000 spectrophotometer (NanoDrop Technologies). All oligonucleotides were PAGE purified prior to the labeling reactions.

VRM Printing and Blocking

Microarray printing was carried out using a Nano-Plotter (NP2.1; GeSiM) on bar-coded Nexterion slide E, epoxysilane-coated substrates (Schott North America). All probes were diluted in spotting buffer (20 mM HEPES, 50 nM KCl, 10 mM MgCl$_2$, 1 mM DTT [pH 7.2]) and spotted at $18 \pm 2^\circ$C and a relative humidity of 50%. Spotting was carried out in one-tip mode with the nano tip A. The average drop volume was 140 pl and 7 drops were deposited for a total of approximately 980 pl/spot. The spotting buffer was also printed on the slides as a negative control. Postprinting, the slides were left in the printer for 30 min to dry before storage at -80°C until use.

VRM Hybridization and Data Analysis

VRM hybridizations were performed between single-stranded, fluorophore-labeled antisense (guide) siRNAs and the HCV replicon RNA under native (non-denaturing) conditions in order to maintain RNA secondary structure. All solutions were prepared with nuclease-free water and all hybridizations were performed at 37°C unless otherwise indicated. All slides were blocked in $4\times$ SSC, 0.1% ultrapure nonacetylated BSA (Ambion) for 15 min at 37°C and washed five times with nuclease-free water at room temperature for 1 min each. The slides were dried prior to the hybridization reaction by centrifugation at $200 \times$ g for 5 min. Hybridizations were performed in $1\times$ Hyb buffer (20 mM HEPES [pH 7.8], 50 mM KCl, 10 mM MgCl$_2$, 1 mM DTT) supplemented with 100 μg/ml yeast tRNAs, 0.625 mg/ml salmon sperm DNA, 40 U RNase-OUT (Invitrogen), 300 pg/μl Cy3-Cj1119c oligonucleotide, 900 pg/μl Cy3-Cj0373 oligonucleotide, 30 nM Cy5-Luc988-42 nt, and 1 μM siRNA in a 40 μl reaction volume. The hybridization reactions were denatured at 65°C for 5 min and then incubated at 37°C for 10 min prior to application to the VRMs. Both the cover-slips and microarray slides were preheated to 37°C for 10 min prior to hybridization. Hybridizations were performed for 45 min to 1 hr at 37°C under glass coverslips (24 $\times$ 20 mm) in a humidified SlideBooster hybridization chamber (Olympus Advalytix). For hybridizations carried out under denaturing conditions, hybridization buffer was replaced with a denaturing 50% DIG Easy Hybridization solution (Roche) and hybridizations (target microarray + hybridization solution) were initially heated to 65°C and slowly cooled to 37°C over the 1 hr hybridization period. After hybridization, microarrays were washed twice with $1\times$ SSC + 0.05% SDS, twice with $0.5\times$ SSC, and twice with $0.1\times$ SSC at 45°C for 5 min each. The slides were spun dry by centrifugation at $200 \times$ g for 5 min and stored in light-tight containers until they were scanned. VRMs were scanned using the VersArray Chipreader (Bio-Rad) according to the recommendations of the manufacturer.

Spot quantification, signal normalization, and data analysis were performed using Array-Pro Analyzer image analysis software (version 4.5; MediaCybernetics). Net signal intensities were obtained by local-ring background subtraction (net intensity = raw intensity – background). For normalization purposes and to account for spot morphology, the ratio of the signal intensities of the siRNAs (Cy3 channel) to that of the Luc988-42 nt normalization control (Cy5 channel) of the spots containing HCV RNA was used for further analysis (normalized net intensity). The Cy3-labeled *C. jejuni* oligonucleotides were used to scale the intensities between microarrays. A single HCV replicon RNA concentration was chosen for analysis (125 ng/μl) because it had a greater than 2-fold signal-to-noise ratio without reaching saturation for all HCV-specific siRNAs. Signal intensities for quadruplicate spots were averaged, and all hybridizations were carried out in duplicate or triplicate.

In Vitro Hybridizations for VRBs

One microgram of biotinylated HCV subgenomic replicon RNA was diluted in $1\times$ hybridization buffer (20 mM HEPES [pH 7.8], 50 mM KCl, 10 mM MgCl$_2$, 1 mM DTT) supplemented with 0.625 mg/ml salmon sperm DNA, 50 μg/ml yeast tRNA, and 0.2 U/μl SUPER-In RNase Inhibitor (Ambion) in a total volume of 20 μl. The siRNAs were diluted to final concentrations ranging from 0.01 to 1 μM. Hybridizations were then carried out at 37°C for 30 min. For hybridizations carried out under denaturing conditions, the samples were prepared as described above, except the reactions were first heat denatured at 80°C for 15 min, followed by incubation on ice for 2 min, prior to hybridization at 37°C for 30 min. In order to account for background binding of siRNA to the beads, control reactions were carried out in the absence of HCV subgenomic replicon RNA.

Magnetic Microbead Preparation and Immobilization of RNA for VRBs

Approximately 5 $\times$ 10^6 streptavidin-coated Dynabeads M-280 (Invitrogen) were used per sample. After resuspension, beads were washed three times with $1\times$ B&W buffer ($2\times$ B&W buffer: 10 mM Tris-HCl [pH 7.5], 2 M NaCl) and then washed twice with solution A (0.1 M NaOH, 0.05 M NaCl) at room temperature. Finally, the beads were washed twice with hybridization buffer at room temperature prior to incubation with the hybridization reactions.

The in vitro hybridization reactions in solution were then added to the strep-tavidin-coated Dynabeads and were then incubated at 37°C for 20 min to capture the biotinylated HCV subgenomic replicon RNAs. After immobilization, the VRBs were washed twice with $2\times$ SSC and twice with $1\times$ SSC, and resuspended in 10 μl of RNase-free PBS. The beads were visualized by fluorescence using an Olympus BX51 fluorescent microscope (Olympus Optical). All hybridization reactions were carried out in triplicate.

VRB Image and Data Analysis

The quantification of signal intensities from the VRBs was performed using Image-Pro Plus 4.5 software (Media Cybernetics) by calculating the integrated optical density (IOD) from individual beads. Net signal intensities were obtained by local-ring background subtraction (net = raw – background). The net signal intensity for each bead was then normalized to the area of the bead (net IOD/area) and averaged for approximately 100 beads per image.

For normalization purposes, the net IODs from the control hybridization reactions carried out in the absence of HCV subgenomic replicon RNA were subtracted from the net IODs. For each siRNA, hybridization experiments conducted using native HCV RNA and HCV RNA that was heat denatured during hybridization (80°C) were carried out at final siRNA concentrations ranging from 0.01 to 1 μM. From these hybridizations, standard curves for native and denatured HCV RNA were generated from linear least-squares fitting of the net IODs versus siRNA concentration in each case. Target site accessibility was assessed by the ratio of the slope of the siRNA hybridization to native HCV RNA over the slope of the siRNA hybridization to denatured HCV RNA.

Western Blot Analysis

For detection of HCV proteins, whole-cell lysates were prepared from Huh-7 cells harboring subgenomic replicons after treatment with siRNAs as described for 24, 48, or 72 hr. Cells were washed twice with PBS and lysed with a lysis buffer consisting of 50 mM Tris-HCl (pH 6.8), 2% SDS, 10% glycerol, 100 mM DTT, and 0.1% bromophenol blue (prepared initially without the DTT and bromophenol blue). Complete protease inhibitor cocktail (Roche Diagnostics) was added to each extract to a final concentration of $1\times$. The protein concentration of each sample was quantified using the Bio-Rad DC protein assay according to the manufacturer's protocol. Prior to loading, 10% DTT and bromophenol blue (1:1) was added to each sample and the samples were heated to 95°C for 5 min and cooled on ice. Approximately 60 μg of protein per well was loaded for SDS-PAGE (10% resolving, 4% stacking gel). The resolved proteins were transferred to a Hybond-P PVDF membrane (GE Healthcare). The membrane was blocked for 1 hr with 5% skim milk in TBS-Tween and probed for the HCV NS5A protein with a mouse monoclonal anti-NS5A antibody (0.2 μg/ml; Virostat) followed by an HRP-conjugated goat anti-mouse IgG antibody (1:1000 dilution; Jackson ImmunoResearch Laboratories). As a loading control, the membranes were stripped using Re-blot Plus Strong Solution (Millipore) according to the manufacturer's protocol, and reprobed with a mouse anti-PTP1D/SHP2 primary antibody (1:1000 dilution; Sigma) with the same secondary antibody as described above. Protein bands were visualized by using Western Lightning western blot chemiluminescence reagents (PerkinElmer) according to the manufacturer's protocol.

RNA Isolation and Northern Blot Analysis

Total RNA was isolated from siRNA-transfected HCV subgenomic replicon-harboring cells at 24, 48, and 72 hr posttransfection using the RNeasy extraction kit (QIAGEN). Approximately 0.5 μg/well of total RNA was loaded onto a 1% agarose gel. Biotinylated negative-sense probes complementary to the HCV genome NS5B region nt 6648–7770 (GenBank accession number AJ242654) and the β-actin gene (GenBank accession number X00351) were synthesized using the MEGAscript T7 kit (Ambion). In vitro transcriptions were performed as described above with the inclusion of biotin-11-UTP and

biotin-11-CTP (PerkinElmer) at a molar ratio of 1:3 with unlabeled UTP and unlabeled CTP, respectively, and were carried out at 37°C overnight. DNA template was removed by DNase I digestion, and biotinylated RNA was purified using the MEGAclear kit (Ambion) with elution in RNase-free water. The biotinylated negative-sense probes were used at a final concentration of 2.2 ng/μl and 0.133 ng/μl for the HCV and β-actin probes, respectively. Northern blotting and hybridization were carried out using the NorthernMAX kit (Ambion) and Hybond XL nylon membranes (GE Healthcare). The bound riboprobes were detected using the Chemiluminescent Nucleic Acid Detection Module (Pierce) according to the manufacturer's protocol.

Quantitative PCR

For quantitative PCR (qPCR) analyses, Huh-7 cells harboring subgenomic replicons were treated with siRNAs as described. At 24 hr posttransfection, total RNA was isolated using the RNeasy extraction kit (QIAGEN), followed by a 30 min digestion with DNase I (Ambion). Total RNA was then purified with the DNA-free kit (Ambion). The concentration was determined by measurement of the absorbance at 260 nm with an ND-1000 spectrophotometer (NanoDrop Technologies), and RNA integrity was verified by agarose gel electrophoresis. Five hundred nanograms of total RNA was used for cDNA synthesis using the Superscript II kit (Invitrogen) according to the manufacturer's protocol. Quantitative PCR was performed on an iCycler (Bio-Rad) using Platinum SYBR Green Supermix (Invitrogen) containing 20 nM fluorescein (Bio-Rad) with primers directed against the HCV IRES region (5′-GTC TGC GGA ACC GGT GAG TA-3′ and 5′-GCC CAA ATC TCC AGG CAT T-3′), and 18S rRNA (5′-GCG ATG CGG CGG CGT TAT TC-3′ and 5′-CAA TCT GTC AAT CCT GTC CGT GTC C-3′) and GAPDH (5′-AGG CTG TGG GCA AGG TCA TCC-3′ and 5′-AGT GGG TGT CGC TGT TGA AGT CA-3′) were used as reference genes. A 20 μl reaction was assembled according to the manufacturer's protocol. For data analysis, the $2^{-\Delta\Delta Ct}$ method was used (Livak and Schmittgen, 2001), and mean fold changes relative to untreated HCV subgenomic replicon RNA-harboring cells are presented. Each qPCR experiment was carried out in triplicate.

Data Sets and Bioinformatic Methods

The sequence data set used for hepacivirus analyses was created by Dr. Peter Simmonds using the Simmonic Sequence Editor version 1.6 (http://www.picornavirus.org/software) (Simmonds and Smith, 1999; Simmonds et al., 2004; Davis et al., 2008) from complete genome sequences downloaded from GenBank. The 83 published HCV genotype 1b sequences were used for the bioinformatics analyses.

MFEs were calculated for consecutive 150-base fragments (in 2-base increments) of each sequence from each alignment using the folding energy scan in the Simmonic Sequence Editor program from a locally compiled copy of UNA-Fold (Markham and Zuker, 2005) running on Windows XP. For each sequence, MFE differences from the null expectation (MFED) (Workman and Krogh, 1999; Davis et al., 2008) were calculated by the parallel submission of 50 sequence scrambles using the NDR algorithm in the Simmonic Sequence Editor, which retains dinucleotide frequency biases (Simmonds et al., 2004; Davis et al., 2008). Results are expressed as MFEDs (i.e., the % difference in MFEs of native and scrambled sequences, calculated as {[(MFE$_{Native}$/MFE$_{Scrambled}$) − 1] × 100} (Workman and Krogh, 1999; Davis et al., 2008).

REFERENCES

Alvarez, D.E., Lodeiro, M.F., Luduena, S.J., Pietrasanta, L.I., and Gamarnik, A.V. (2005). Long-range RNA-RNA interactions circularize the dengue virus genome. J. Virol. 79, 6631–6643.

Blight, K.J., and Rice, C.M. (1997). Secondary structure determination of the conserved 98-base sequence at the 3′ terminus of hepatitis C virus genome RNA. J. Virol. 71, 7345–7352.

Bohula, E.A., Salisbury, A.J., Sohail, M., Playford, M.P., Riedemann, J., Southern, E.M., and Macaulay, V.M. (2003). The efficacy of small interfering RNAs targeted to the type 1 insulin-like growth factor receptor (IGF1R) is influenced by secondary structure in the IGF1R transcript. J. Biol. Chem. 278, 15991–15997.

Brown, K.M., Chu, C.Y., and Rana, T.M. (2005). Target accessibility dictates the potency of human RISC. Nat. Struct. Mol. Biol. 12, 469–470.

Davis, M., Sagan, S.M., Pezacki, J.P., Evans, D.J., and Simmonds, P. (2008). Bioinformatic and physical characterizations of genome-scale ordered RNA structure in mammalian RNA viruses. J. Virol. 82, 11824–11836.

Diviney, S., Tuplin, A., Struthers, M., Armstrong, V., Elliott, R.M., Simmonds, P., and Evans, D.J. (2008). A hepatitis C virus cis-acting replication element forms a long-range RNA-RNA interaction with upstream RNA sequences in NS5B. J. Virol. 82, 9008–9022.

Drygin, Y.F., Bordunova, O.A., Gallyamov, M.O., and Yaminsky, I.V. (1998). Atomic force microscopy examination of tobacco mosaic virus and virion RNA. FEBS Lett. 425, 217–221.

Elbashir, S.M., Harborth, J., Weber, K., and Tuschl, T. (2002). Analysis of gene function in somatic mammalian cells using small interfering RNAs. Methods 26, 199–213.

Fire, A., Xu, S.Q., Montgomery, M.K., Kostas, S.A., Driver, S.E., and Mello, C.C. (1998). Potent and specific genetic interference by double-stranded RNA in Caenorhabditis elegans. Nature 391, 806–811.

Friebe, P., and Bartenschlager, R. (2002). Genetic analysis of sequences in the 3′ nontranslated region of hepatitis C virus that are important for RNA replication. J. Virol. 76, 5326–5338.

Friebe, P., Lohmann, V., Krieger, N., and Bartenschlager, R. (2001). Sequences in the 5′ nontranslated region of hepatitis C virus required for RNA replication. J. Virol. 75, 12047–12057.

Friebe, P., Boudet, J., Simorre, J., and Bartenschlager, R. (2005). Kissing-loop interaction in the 3′ end of the hepatitis C virus genome essential for RNA replication. J. Virol. 79, 380–392.

Giro, A., Bergia, A., Zuccheri, G., Bink, H.H., Pleij, C.W., and Samori, B. (2004). Single molecule studies of RNA secondary structure: AFM of TYMV viral RNA. Microsc. Res. Tech. 65, 235–245.

Hansma, H.G., Golan, R., Hsieh, W., Daubendiek, S.L., and Kool, E.T. (1999). Polymerase activities and RNA structures in the atomic force microscope. J. Struct. Biol. 127, 240–247.

Hansma, H.G., Oroudjev, E., Baudrey, S., and Jaeger, L. (2003). TectoRNA and 'kissing-loop' RNA: atomic force microscopy of self-assembling RNA structures. J. Microsc. 212, 273–279.

Hansma, H.G., Kasuya, K., and Oroudjev, E. (2004). Atomic force microscopy imaging and pulling of nucleic acids. Curr. Opin. Struct. Biol. 14, 380–385.

Heale, B.S.E., Soifer, H.S., Bowers, C., and Rossi, J.J. (2005). siRNA target site secondary structure predictions using local stable substructures. Nucleic Acids Res. 33, e30.

Hofacker, I.L. (2007). How microRNAs choose their targets. Nat. Genet. 39, 1191–1192.

Holen, T., Amarzguioui, M., Wiiger, M.T., Babaie, E., and Prydz, H. (2002). Positional effects of short interfering RNAs targeting the human coagulation trigger Tissue Factor. Nucleic Acids Res. 30, 1757–1766.

Kedde, M., Strasser, M.J., Boldajipour, B., Oude Vrielink, J.A., Slanchev, K., le Sage, C., Nagel, R., Voorhoeve, P.M., van Duijse, J., Orom, U.A., et al. (2007). RNA-binding protein Dnd1 inhibits microRNA access to target mRNA. Cell 131, 1273–1286.

Kertesz, M., Iovino, N., Unnerstall, U., Gaul, U., and Segal, E. (2007). The role of site accessibility in microRNA target recognition. Nat. Genet. *39*, 1278–1284.

Khvorova, A., Reynolds, A., and Jayasena, S.D. (2003). Functional siRNAs and miRNAs exhibit strand bias. Cell *115*, 209–216.

Kim, Y.K., Kim, C.S., Lee, S.H., and Jang, S.K. (2002). Domains I and II in the 5′ nontranslated region of the HCV genome are required for RNA replication. Biochem. Biophys. Res. Commun. *290*, 105–112.

Kolykhalov, A.A., Feinstone, S.M., and Rice, C.M. (1996). Identification of a highly conserved sequence element at the 3′ terminus of hepatitis C virus genome RNA. J. Virol. *70*, 3363–3371.

Kretschmer-Kazemi Far, R., and Sczakiel, G. (2003). The activity of siRNA in mammalian cells is related to structural target accessibility: a comparison with antisense oligonucleotides. Nucleic Acids Res. *31*, 4417–4424.

Kuznetsov, Y.G., Daijogo, S., Zhou, J., Semler, B.L., and McPherson, A. (2005). Atomic force microscopy analysis of icosahedral virus RNA. J. Mol. Biol. *347*, 41–52.

Le, S.Y., Sonenberg, N., and Maizel, J.V., Jr. (1995). Unusual folding regions and ribosome landing pad within hepatitis C virus and pestivirus RNAs. Gene *154*, 137–143.

Lee, H., Shin, H., Wimmer, E., and Paul, A.V. (2004). *cis*-acting RNA signals in the NS5B C-terminal coding sequence of the hepatitis C virus genome. J. Virol. *78*, 10865–10877.

Lewis, B.P., Shih, I.H., Jones-Rhoades, M.W., Bartel, D.P., and Burge, C.B. (2003). Prediction of mammalian microRNA targets. Cell *115*, 787–798.

Liu, Z., Li, Z., Zhou, H., Wei, G., Song, Y., and Wang, L. (2005). Imaging DNA molecules on mica surface by atomic force microscopy in air and in liquid. Microsc. Res. Tech. *66*, 179–185.

Livak, K.J., and Schmittgen, T.D. (2001). Analysis of relative gene expression data using real-time quantitative PCR and the $2^{-\Delta\Delta CT}$ method. Methods *25*, 402–408.

Lohmann, V., Korner, F., Koch, J., Herian, U., Theilmann, L., and Bartenschlager, R. (1999). Replication of subgenomic hepatitis C virus RNAs in a hepatoma cell line. Science *285*, 110–113.

Long, D., Lee, R., Williams, P., Chan, C.Y., Ambros, V., and Ding, Y. (2007). Potent effect of target structure on microRNA function. Nat. Struct. Mol. Biol. *14*, 287–294.

Luo, K.Q., and Chang, D.C. (2004). The gene-silencing efficiency of siRNA is strongly dependent on the local structure of mRNA at the targeted region. Biochem. Biophys. Res. Commun. *318*, 303–310.

MacRae, I.J., Ma, E., Zhou, M., Robinson, C.V., and Doudna, J.A. (2008). In vitro reconstitution of the human RISC-loading complex. Proc. Natl. Acad. Sci. USA *105*, 512–517.

Manche, L., Green, S.R., Schmedt, C., and Mathews, M.B. (1992). Interactions between double-stranded RNA regulators and the protein kinase DAI. Mol. Cell. Biol. *12*, 5238–5248.

Markham, N.R., and Zuker, M. (2005). DINAMelt web server for nucleic acid melting prediction. Nucleic Acids Res. *33*, W577–W581.

Martinez, J., Patkaniowska, A., Urlaub, H., Luhrmann, R., and Tuschl, T. (2002). Single-stranded antisense siRNAs guide target RNA cleavage in RNAi. Cell *110*, 563–574.

McHutchison, J.G., Bartenschlager, R., Patel, K., and Pawlotsky, J.M. (2006). The face of future hepatitis C antiviral drug development: recent biological and virologic advances and their translation to drug development and clinical practice. J. Hepatol. *44*, 411–421.

McMullan, L.K., Grakoui, A., Evans, M.J., Mihalik, K., Puig, M., Branch, A.D., Feinstone, S.M., and Rice, C.M. (2007). Evidence for a functional RNA element in the hepatitis C virus core gene. Proc. Natl. Acad. Sci. USA *104*, 2879–2884.

Minks, M.A., West, D.K., Benvin, S., and Baglioni, C. (1979). Structural requirements of double-stranded RNA for the activation of 2′,5′-oligo(A) polymerase and protein kinase of interferon-treated HeLa cells. J. Biol. Chem. *254*, 10180–10183.

Noestheden, M., Hu, Q.Y., Tonary, A.M., Tay, L.L., and Pezacki, J.P. (2007). Evaluation of chemical labeling strategies for monitoring HCV RNA using vibrational microscopy. Org. Biomol. Chem. *5*, 2380–2389.

Obernosterer, G., Tafer, H., and Martinez, J. (2008). Target site effects in the RNA interference and microRNA pathways. Biochem. Soc. Trans. *36*, 1216–1219.

Overhoff, M., Alken, M., Far, R.K.K., Lemaitre, M., Lebleu, B., Sczakiel, G., and Robbins, I. (2005). Local RNA target structure influences siRNA efficacy: a systematic global analysis. J. Mol. Biol. *348*, 871–881.

Randall, G., Grakoui, A., and Rice, C.M. (2003). Clearance of replicating hepatitis C virus replicon RNAs in cell culture by small interfering RNAs. Proc. Natl. Acad. Sci. USA *100*, 235–240.

Reynolds, A., Leake, D., Boese, Q., Scaringe, S., Marshall, W.S., and Khvorova, A. (2004). Rational siRNA design for RNA interference. Nat. Biotechnol. *22*, 326–330.

Rivetti, C., Guthold, M., and Bustamante, C. (1996). Scanning force microscopy of DNA deposited onto mica: equilibration versus kinetic trapping studied by statistical polymer chain analysis. J. Mol. Biol. *264*, 919–932.

Schubert, S., Grunweller, A., Erdmann, V.A., and Kurreck, J. (2005). Local RNA target structure influences siRNA efficacy: systematic analysis of intentionally designed binding regions. J. Mol. Biol. *348*, 883–893.

Schwarz, D.S., Hutvagner, G., Du, T., Xu, Z.S., Aronin, N., and Zamore, P.D. (2003). Asymmetry in the assembly of the RNAi enzyme complex. Cell *115*, 199–208.

Simmonds, P. (2004). Genetic diversity and evolution of hepatitis C virus—15 years on. J. Gen. Virol. *85*, 3173–3188.

Simmonds, P., and Smith, D.B. (1999). Structural constraints on RNA virus evolution. J. Virol. *73*, 5787–5794.

Simmonds, P., Tuplin, A., and Evans, D.J. (2004). Detection of genome-scale ordered RNA structure (GORS) in genomes of positive-stranded RNA viruses: implications for virus evolution and host persistence. RNA *10*, 1337–1351.

Srisawat, C., and Engelke, D.R. (2002). RNA affinity tags for purification of RNAs and ribonucleoprotein complexes. Methods *26*, 156–161.

Tafer, H., Ameres, S.L., Obernosterer, G., Gebeshuber, C.A., Schroeder, R., Martinez, J., and Hofacker, I.L. (2008). The impact of target site accessibility on the design of effective siRNAs. Nat. Biotechnol. *26*, 578–583.

Tanaka, T., Kato, N., Cho, M.J., and Shimotohno, K. (1995). A novel sequence found at the 3′ terminus of hepatitis C virus genome. Biochem. Biophys. Res. Commun. *215*, 744–749.

Tanaka, T., Kato, N., Cho, M.J., Sugiyama, K., and Shimotohno, K. (1996). Structure of the 3′ terminus of the hepatitis C virus genome. J. Virol. *70*, 3307–3312.

Tuplin, A., Wood, J., Evans, D.J., Patel, A.H., and Simmonds, P. (2002). Thermodynamic and phylogenetic prediction of RNA secondary structures in the coding region of hepatitis C virus. RNA *8*, 824–841.

Tuplin, A., Evans, D.J., and Simmonds, P. (2004). Detailed mapping of RNA secondary structures in core and NS5B-encoding region sequences of hepatitis C virus by RNase cleavage and novel bioinformatic prediction methods. J. Gen. Virol. *85*, 3037–3047.

Umemura, K., Nagami, F., Okada, T., and Kuroda, R. (2000). AFM characterization of single strand-specific endonuclease activity on linear DNA. Nucleic Acids Res. *28*, E39.

Varekova, R.S., Bradac, I., Plchut, M., Skrdla, M., Wacenovsky, M., Mahr, H., Mayer, G., Tanner, H., Brugger, H., Withalm, J., et al. (2008). A new program for analyzing RNA interference. Comput. Methods Programs Biomed. *90*, 89–94.

Vickers, T.A., Koo, S., Bennett, C.F., Crooke, S.T., Dean, N.M., and Baker, B.F. (2003). Efficient reduction of target RNAs by small interfering RNA and RNase H-dependent antisense agents. A comparative analysis. J. Biol. Chem. *278*, 7108–7118.

Wang, C., and Siddiqui, A. (1995). Structure and function of the hepatitis C virus internal ribosome entry site. Curr. Top. Microbiol. Immunol. *203*, 99–115.

Wang, C., Le, S.Y., Ali, N., and Siddiqui, A. (1995). An RNA pseudoknot is an essential structural element of the internal ribosome entry site located within the hepatitis C virus 5′ noncoding region. RNA 1, 526–537.

Watts, J.M., Dang, K.K., Gorelick, R.J., Leonard, C.W., Bess, J.W., Jr., Swanstrom, R., Burch, C.L., and Weeks, K.M. (2009). Architecture and secondary structure of an entire HIV-1 RNA genome. Nature 460, 711–716.

Wilson, J.A., and Richardson, C.D. (2005). Hepatitis C virus replicons escape RNA interference induced by a short interfering RNA directed against the NS5b coding region. J. Virol. 79, 7050–7058.

Wilson, J.A., Jayasena, S., Khvorova, A., Sabatinos, S., Rodrigue-Gervais, I.G., Arya, S., Sarangi, F., Harris-Brandts, M., Beaulieu, S., and Richardson, C.D. (2003). RNA interference blocks gene expression and RNA synthesis from hepatitis C replicons propagated in human liver cells. Proc. Natl. Acad. Sci. USA 100, 2783–2788.

Workman, C., and Krogh, A. (1999). No evidence that mRNAs have lower folding free energies than random sequences with the same dinucleotide distribution. Nucleic Acids Res. 27, 4816–4822.

Xu, Y., Zhang, H.Y., Thormeyer, D., Larsson, O., Du, Q., Elmen, J., Wahlestedt, C., and Liang, Z. (2003). Effective small interfering RNAs and phosphorothioate antisense DNAs have different preferences for target sites in the luciferase mRNAs. Biochem. Biophys. Res. Commun. 306, 712–717.

Yiu, S.M., Wong, P.W., Lam, T.W., Mui, Y.C., Kung, H.F., Lin, M., and Cheung, Y.T. (2005). Filtering of ineffective siRNAs and improved siRNA design tool. Bioinformatics 21, 144–151.

Yokota, T., Sakamoto, N., Enomoto, N., Tanabe, Y., Miyagishi, M., Maekawa, S., Yi, L., Kurosaki, M., Taira, K., Watanabe, M., and Mizusawa, H. (2003). Inhibition of intracellular hepatitis C virus replication by synthetic and vector-derived small interfering RNAs. EMBO Rep. 4, 602–608.

You, S., and Rice, C.M. (2008). 3′ RNA elements in hepatitis C virus replication: kissing partners and long poly(U). J. Virol. 82, 184–195.

You, S., Stump, D.D., Branch, A.D., and Rice, C.M. (2004). A cis-acting replication element in the sequence encoding the NS5B RNA-dependent RNA polymerase is required for hepatitis C virus RNA replication. J. Virol. 78, 1352–1366.

Zamore, P.D., and Haley, B. (2005). Ribo-gnome: the big world of small RNAs. Science 309, 1519–1524.